

HUBBLE SPACE TELESCOPE SPECTROSCOPY OF THE DWARF NOVA RX ANDROMEDAE DURING OUTBURST RISE AND DECLINE

JEREMY F. SEPINSKY,¹ EDWARD M. SION,¹ PAULA SZKODY,² AND BORIS T. GÄNSICKE³

Received 2002 March 2; accepted 2002 April 3

ABSTRACT

We obtained *Hubble Space Telescope* far-ultraviolet spectra of the Z Cam–type dwarf nova RX And during the early rise to outburst and the decline from the same outburst. The spectral wavelength range covered was 1149–1435 Å. The rise spectrum is dominated by strong, very broad absorption lines, while the decline spectrum has strong, narrower absorption with weak to moderately strong emission wings due to the presence of disk material. We have carried out a combined model accretion disk and high-gravity model atmosphere analysis of these spectra. The rise spectrum is best fitted to the Ly α region, metal absorption lines, and longward continuum with a model optically thick accretion disk having an accretion rate of $2 \times 10^{-10} M_{\odot} \text{ yr}^{-1}$, a white dwarf of mass $M_{\text{wd}} = 0.8 M_{\odot}$, with $T_{\text{eff}} = 40,000 \text{ K}$, $\log g = 8.2$, and a disk inclination angle of 41° . The hot white dwarf accounts for 62% of the far-UV flux, while the disk accounts for 38%. Our best-fitting multicomponent model of the decline spectrum reveals the presence of a hot (45,000 K) white dwarf contributing 81.4% of the flux during the decline and a remaining accretion disk component with an accretion rate during the decline of 2.85×10^{-10} , contributing 18.6% of the flux. We find that the RX And white dwarf was heated by $\sim 11,000 \text{ K}$ during the outburst. Evolutionary simulations with time-variable accretion indicate that boundary layer irradiation has a larger effect on this heating amplitude than compressional heating.

Subject headings: accretion, accretion disks — novae, cataclysmic variables — stars: individual (RX Andromedae) — ultraviolet: stars — white dwarfs

1. INTRODUCTION

Dwarf novae are an important subset of cataclysmic variables (CVs), which undergo quasi-periodic outbursts identified with the release of gravitational energy when rapid accretion occurs from an accretion disk onto a white dwarf. These extremely close binaries consist of a Roche lobe–filling, main-sequence–like secondary star that transfers matter with angular momentum into a disk surrounding the white dwarf. The luminous outbursts appear to be triggered when the accretion disk suffers a thermal instability, which greatly enhances the rate of accretion of the disk material onto the degenerate star. How this disk gas with its mass, energy, and angular momentum affects the white dwarf is a fundamental question in stellar physics. The advent of far-UV space observation opened the way for studies of the properties of the underlying white dwarf in dwarf novae during dwarf nova quiescence when, in several systems, the accretion-heated white dwarf is detected directly and the far-UV flux contribution of the cool disk is at its minimum (Sion 1999 and references therein).

In many dwarf novae, the outburst durations are variable and the durations of the inter-outburst quiescence intervals are short and unpredictable. It is often a challenge to schedule space observations (see below). In order to study the response of the white dwarf to disk accretion, we obtained three equally spaced spectra of RX And with the hope that at least one *Hubble Space Telescope* (*HST*) observation

would catch the system during quiescence. The result was that we have serendipitously obtained three *HST* spectra at key points in the outburst cycle of RX And. The first spectrum was taken near the end of an anomalously long quiescence and revealed the underlying white dwarf with $T_{\text{eff}} = 34,000 \pm 1000 \text{ K}$, $\log g = 8 \pm 0.3$ as the dominant source (75%) of the far-UV light, with the accretion disk at an inclination of 60° , contributing 25% of the system light (Sion et al. 2001). The accretion rate at the end of the extended quiescence was found to be $3 \times 10^{-11} M_{\odot} \text{ yr}^{-1}$. The second spectrum was taken on the rise to outburst, while the third spectrum was taken on the decline. In this paper we carry out a multicomponent analysis of the remaining two spectra taken on the rise to outburst and the decline from outburst.

2. OBSERVATIONS

Timing *HST* observations to occur during a quiescence of RX And required considerable planning. The outbursts of RX And range from 3 to 10 days, while its quiescence normally ranges from 5 to 20 days. The short timing of the cycle prohibited any target of opportunity status with *HST*. The observing strategy adopted is described in Sion et al. (2001) and will not be repeated here.

The temporal placement of the observations with respect to the outburst and quiescence cycle of RX And is shown in Figure 1, where we present the American Association of Variable Star Observers (AAVSO) light curve data. The first set of observations took place approximately 110 days after the last previous outburst (see Sion et al. 2001), the second set during the rise to outburst, and the third set on the decline from outburst.

The observations for visits 2 (rise) and 3 (decline) were carried out in the ACCUM mode with the D2 detector of

¹ Department of Astronomy and Astrophysics, Villanova University, Villanova, PA 19085; jeremy@ast.villanova.edu, emsion@ast.villanova.edu.

² Department of Astronomy, University of Washington, Box 351580, Seattle, WA 98195; szkody@alicer.astro.washington.edu.

³ Department of Physics and Astronomy, University of Southampton, Highfield, Southampton S017 1BJ, UK; btg@astro.soton.ac.uk.

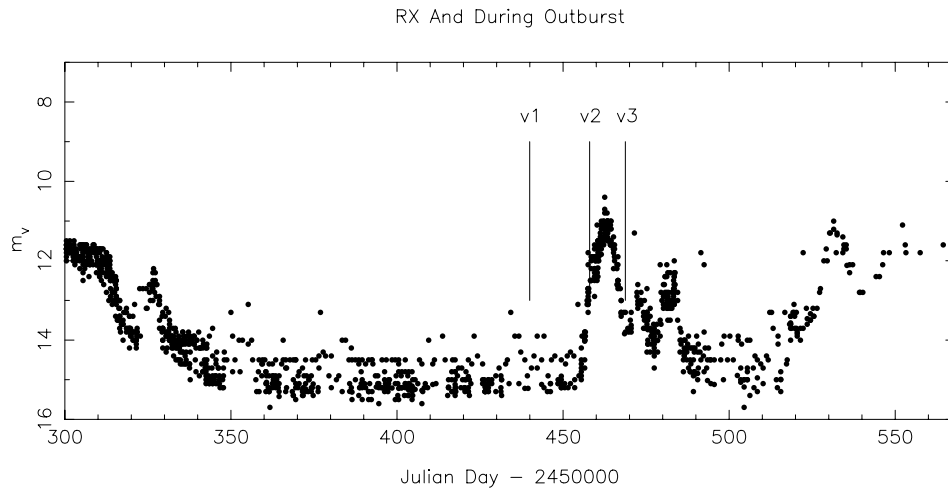


FIG. 1.—AAVSO light curve for RX And during the *HST* GHRS observations. The placement of the *HST* observations for each of the three visits is indicated. Note the extraordinarily long quiescent interval of RX And.

the Goddard High Resolution Spectrograph (GHRS) and the G140L disperser. The wavelength coverage was 1149.184–1435.492 Å with a spectral resolution of 0.21 Å and a time resolution of 58.5 s. The details of the observations are given in Table 1, where we have listed the start time of the observations, the total exposure time in seconds, and the orbital phase at the start and end of the total exposure. The orbital phase range in Table 1 was computed by using the best available orbital ephemeris due to Kaitchuk (1989) as follows: $2447041.932 \pm 0.2098930E \pm 0.002$. In this phase convention, the white dwarf would have maximum positive velocity at phase 0.75 and maximum negative velocity at phase 0.25.

Spectra 2 and 3 are displayed in Figure 2 in the middle and bottom panels, respectively. In the top panel, the spectrum in quiescence analyzed by Sion et al. (2001) is displayed for easy comparison of relative flux changes and line profile variations at the three different times in the outburst cycle.

3. SYNTHETIC SPECTRUM ANALYSIS

In order to model the spectra of RX And and estimate the white dwarf and disk properties during the rise to and decline from outburst, we constructed a grid of model stellar atmosphere spectra under local thermodynamic equilibrium (LTE) with TLUSTY (Hubeny 1988; Hubeny & Lanz 1995) and SYNSPEC (Hubeny, Lanz, & Jeffery 1994), with solar abundance. We incorporated optically thick, steady state disk models from the extensive grid of Wade & Hubeny (1998). No interstellar reddening correction was applied, as this value has been shown to be very low (Verbunt 1987).

TABLE 1
HST GHRS OBSERVATIONS OF RX AND

NUMBER	OBSERVATION DATE	OBSERVATION TIME	TOTAL EXPOSURE (s)	ORBITAL PHASE	
				Start	End
2.....	1997 Jan 9	11:41:52	1142.4	0.223	0.291
3.....	1997 Jan 20	06:33:20	1142.4	0.610	0.678

To analyze the spectrum on the rise to outburst, we began by assuming that the disk is the only contributor to the far-UV continuum. This assumption is validated by the disk instability model of a dwarf nova outburst which holds that the outburst is due to an increase in the luminosity of the disk caused by collapse onto the white dwarf (Cannizzo 1998). Since this spectrum was taken on the rise to outburst, it was possible that the disk luminosity increase could be the majority, if not the only, flux contribution to the outburst. We determined that the best fit for the rise spectrum corresponded to an accretion rate of $10^{-10} M_{\odot} \text{ yr}^{-1}$, for a white dwarf mass of $0.8 M_{\odot}$, with a disk inclination angle of 41° . The model yielded a χ^2 of 3.26 and showed good agreement in the absorption features, but evidenced a flux discrepancy along the longward portion of the continuum. The best-fitting accretion disk model for the rise spectrum is shown in Figure 3.

In an effort to improve the fit to the rise spectrum, particularly the agreement between the model and the observed continua, a disk model with an accretion rate of $10^{-10} M_{\odot} \text{ yr}^{-1}$ and $i = 41^{\circ}$ was combined with a grid of white dwarf models having temperatures of 30,000–50,000 K in steps of 1000 K, with solar abundances. This model accretion rate was modified by small increments between 0.1 and 10 times the model rate using our routine WDDISKFIT until the minimum χ^2 fit was achieved in the white dwarf plus disk fits. The best fit occurred for $T_{\text{eff}} = 40,000$ K, $\dot{M} = 2 \times 10^{-10} M_{\odot} \text{ yr}^{-1}$, $M = 0.8 M_{\odot}$, and $i = 41^{\circ}$, with a $\chi^2 = 1.517$ and a scale factor distance of 191 pc. In this fit, the white dwarf contributes 62% of the flux and the disk contributes 38%. This best fit to the rise spectrum is shown in Figure 4. The C and Si abundances were enhanced to 5 and 10 times solar, respectively, in order to reach better agreement with the observed line strengths.

To analyze the spectrum on the decline from outburst, we began by fitting the observed data with disk and photosphere models individually. Each of the fitted models showed a significant shortfall from the continuum flux levels, even though the model line profiles resembled the shapes of the observed absorption lines. This led us to consider a more in-depth and, indeed, more realistic composite model that incorporated a combination of both components.

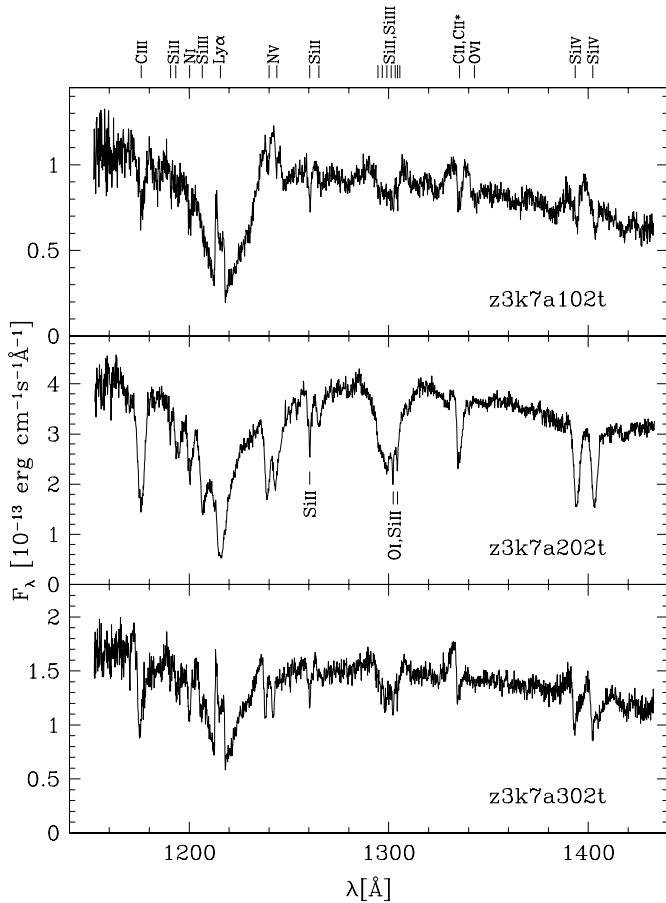


FIG. 2.—*Top*: GHRSL spectrum of RX And (flux F_λ vs. wavelength) for the first observation (late anomalous quiescence). Note the very broad Stark-broadened Ly α absorption with narrow airglow emission and the rich metallic absorption line spectrum, with the strongest lines of Si II, Si III, Si IV, C II, and C III labeled in the spectrum. *Middle*: The flux F_λ vs. wavelength for the second observation (rise to outburst). Note the dominance of much stronger, very broad absorption including the great strengthening of N V and Si III. The flux level of this spectrum is the highest of the three summed spectra. *Bottom*: The flux F_λ vs. wavelength for spectrum 3 (decline from outburst). Note the very broad Stark-broadened Ly α absorption with narrow airglow emission, the rich but weakened metallic absorption line spectrum, with the strongest lines being Si II ($\lambda 1260$) Si III ($\lambda 1298$), C II ($\lambda 1335$), and C III ($\lambda 1175$). Note the weaker N V features and the possible longward “red” asymmetric inverse P Cygni profiles in C III ($\lambda 1175$), N V ($\lambda \lambda 1238, 1242$), C II ($\lambda 1335$), and Si IV ($\lambda \lambda 1393, 1402$).

In addition to using the Wade & Hubeny (1998) grid of disk models, we constructed a three parameter grid of high-gravity photosphere models with varying V_{rot} , $\log g$, and T_{wd} . The V_{rot} ranged from 200 to 600 km s $^{-1}$ in steps of 100 km s $^{-1}$, the $\log g$ had values of 7.5, 8.0, and 8.5, and T_{wd} ranged from 34,000 to 48,000 K in steps of 1000 K. From this parameter range, we find a white dwarf of mass $0.8 M_\odot$, with a $V_{\text{rot}} = 200$ km s $^{-1}$, $\log g = 8.22$, $T_{\text{eff}} = 45,000$ K, along with an accretion rate of $\dot{M} = 2.9 \times 10^{-10}$ and an inclination of $i = 60^\circ$, yields the best-fitting model, resulting in a χ^2 of 1.00053. The model showed a contribution of 81.4% from the white dwarf and 18.6% from the disk, as predicted by our initial assumptions of the outburst properties, thus supporting these assumptions. The best-fitting white dwarf plus accretion disk composite model is displayed in Figure 5.

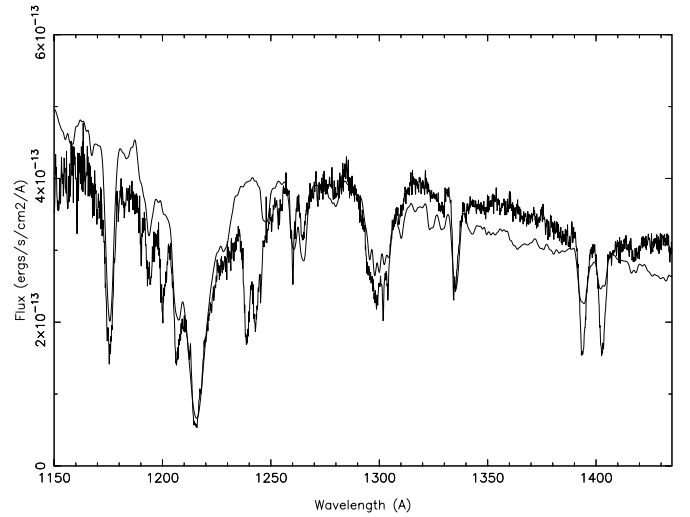


FIG. 3.—GHRSL spectrum taken on the rise to outburst. The best-fitting accretion disk model corresponding to $\dot{M} = 1 \times 10^{-10} M_\odot \text{ yr}^{-1}$, $M = 0.8 M_\odot$, and $i = 41^\circ$ is shown for comparison. The fit to the Ly α region is satisfactory, but the longward continuum is not represented well.

In both visits 2 and 3, the derivation of individual element abundances is complicated by multicomponent contributions to absorption (visit 2) and by emission wings and reversals (visit 3). In the spectrum on the rise to outburst, the strong broad absorption features are identified with the velocity broadening expected in the inner disk. Although our disk model does not incorporate variable chemical abundances, using fixed solar abundances for all elements, the model lines differ significantly from the observed absorption strengths. By enhancing the abundances of C and Si above solar, better agreement was achieved with the observed absorption.

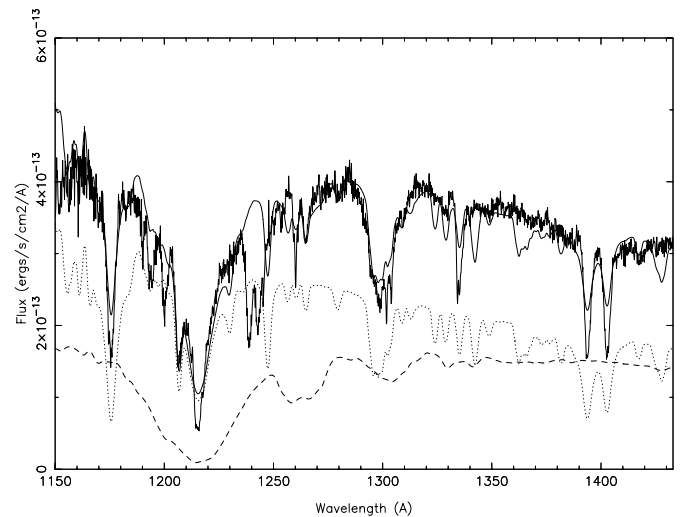


FIG. 4.—GHRSL spectrum taken on the rise to outburst. The top solid curve is the best-fitting combination, the dotted curve is the white dwarf spectrum alone, and the dashed curve is the accretion disk synthetic spectrum alone. The best fit occurred for $T_{\text{eff}} = 40,000$ K, $\dot{M} = 2 \times 10^{-10} M_\odot \text{ yr}^{-1}$, $M = 0.8 M_\odot$, and $i = 41^\circ$, with a $\chi^2 = 1.517$ and a scale factor distance of 191 pc. In this fit, the white dwarf contributes 62% of the flux and the disk contributes 38%.

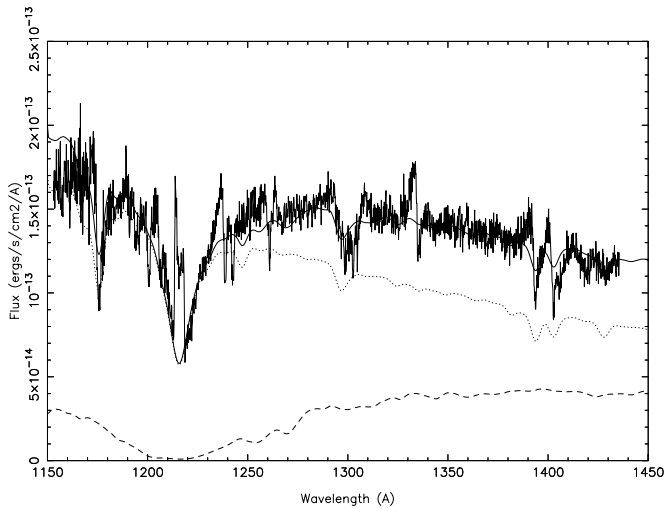


FIG. 5.—Best-fit combination of white dwarf plus accretion disk synthetic fluxes to the decline spectrum. The best-fit occurred for $T_{\text{eff}} = 45,000$ K, $\dot{M} = 2.85 \times 10^{-10} M_{\odot} \text{ yr}^{-1}$, $M = 0.8 M_{\odot}$, and $i = 60^{\circ}$. The top solid curve is the best-fitting combination, the dotted curve is the white dwarf spectrum alone, and the dashed curve is the accretion disk synthetic spectrum alone. In this fit, the white dwarf contributes 81% of the flux and the accretion disk contributes 19%.

In the decline spectrum, the presence of emission wings and the uncertain emission filling of the absorption lines, which could mimic lower abundances, prevent any reliable photospheric metal abundances from being derived. However, it would appear likely that the Si and C abundances are not inconsistent with being solar.

4. CONCLUSIONS

We have modeled the spectroscopic evolution of the RX And system during the rise to an outburst peak and during the decline from the same outburst. We have used multi-component theoretical models combining high-gravity solar composition photospheres with steady state accretion disk models with variable inclination, white dwarf mass, and accretion rate. This investigation, coupled with the analysis of the RX And *HST* spectrum at the end of an unusually long quiescence just preceding the outburst studied here (Sion et al. 2001), represents, to our knowledge, the first far-UV coverage of a nearly complete outburst-quiescence cycle with realistic theoretical multispectral component models.

The spectrum on the rise to outburst is best represented by a combined hot white dwarf (40,000 K) together with a steady state disk model with solar abundances, an inclination of 41° , a white dwarf mass of $0.8 M_{\odot}$, and an accretion rate during the rise of $2 \times 10^{-10} M_{\odot} \text{ yr}^{-1}$. The agreement between the model line profiles and the velocity-broadened absorption features associated with the inner disk confirm that the abundances in the disk cannot be very different from solar. Furthermore, we see no evidence of the extremely sharp line cores such as those seen with *HST* (Huang et al. 1996) during the superoutburst of VW Hydri.

Our best-fitting composite model of the decline spectrum reveals the presence of a hot (45,000 K) white dwarf contributing 81.4% of the flux during the decline and a remaining accretion disk component with an accretion rate during the decline of 2.85×10^{-10} , contributing 18.6% of the flux. This rate of accretion is nearly an order of magnitude larger than

the rate determined by Sion et al. (2001) for the extended quiescence spectrum just preceding the outburst. Without the disk contribution, we found that a single-temperature white dwarf model did not fit the spectrum well (a flux excess shortward of $\text{Ly}\alpha$ and poor agreement with the longward continuum). The inclusion of a disk contribution of 18% brought the observations and models into very good agreement.

The white dwarf during the decline is hotter by 11,000 K than its surface temperature at the end of the long quiescence (Sion et al. 2001). This would indicate that the white dwarf was heated substantially by the outburst. The heating was almost certainly due to the combined effect of boundary layer irradiation (Pringle 1988), compressional heating due to the weight of the added matter (Sion 1995), and shear mixing luminosity due to the conversion of rotational kinetic energy into heat during the tangential disk accretion (Sparks et al. 1993). The cooling by 11,000 K from the maximum heating of the white dwarf at the peak of the outburst to a lower temperature in early quiescence is consistent with the theoretical results of Sion (1995), who carried out evolutionary model sequences of white dwarfs undergoing time-variable accretion that simulated cyclic dwarf novae outbursts. New evolutionary accreting white dwarf model simulations, which greatly extend the grid of time-variable accretion models published by Sion (1995), are directly applicable to RX And. For a $0.8 M_{\odot}$ white dwarf accreting at $10^{-8} M_{\odot} \text{ yr}^{-1}$ for 3 days, compressional heating alone causes the white dwarf temperature to increase by 5000 K. The model sequence 4h in the grid of Godon & Sion (2002) appears to be most directly applicable to the case of RX And. When boundary layer irradiation is included (with a rotational velocity of 40% Keplerian for the white dwarf), then the white dwarf temperature increases by nearly 15,000 K. Since the RX And white dwarf was heated by at least 10,000 K during the outburst and is rotating below 40% Keplerian, then compressional heating may be the dominant mechanism. Since boundary layer heating occurs in the much thinner and diffuse atmosphere of the white dwarf, its effects are evident on a shorter timescale than those of compressional heating. Therefore, by the time of spectrum 3 (decline from outburst), we expect the boundary layer to have cooled significantly, leaving a residual temperature increase due primarily to compressional heating.

We also note that the amount of heating of the RX And white dwarf between decline and early quiescence is remarkably similar to the elevation of temperature found with the *Far Ultraviolet Spectroscopic Explorer* for U Gem's white dwarf (Froning et al. 2001) during its decline. During the decline from outburst in U Gem, Froning et al. (2001) found $T_{\text{eff}} = 45,000$ K, while in early quiescence the white dwarf had a $T_{\text{eff}} = 37,000$ K.

Some of the line features in spectrum 3 appear to be longward asymmetric (i.e., asymmetric on the “red” side) with emission on the shortward side. The impression is that disk material during the decline of the outburst has a net inward flow onto the white dwarf. If these structures do represent inverse P Cygni features, then the infall velocity of the disk-associated or outburst-associated material can be estimated from measurements of the profiles. The terminal velocity derived from the C II feature is $\sim 469 \text{ km s}^{-1}$, while we measure terminal velocities of ~ 781 and $\sim 592 \text{ km s}^{-1}$ from the N V and Si IV lines, respectively. It is possible that the “inward-flowing” gas was ejected by RX And through

wind outflow during the outburst, but may not have achieved escape velocity and, hence, is observed to be returning to the white dwarf. Similar inverse P Cygni structures were also seen in the sharp line cores in one of two *HST* spectra of VW Hyi's superoutburst (Huang et al. 1996). If the line features in the spectrum of visit 3 are really inverse P Cygni features, then we believe this is the first direct detection of actual gas infall onto the white dwarf in a cataclysmic variable.

We acknowledge with gratitude the support of this work by NASA through grant GO 6700.01-96A (to Villanova University) from the Space Telescope Science Institute, which is operated by the Association of Universities for Research in Astronomy, Inc., under NASA contract NAS 5-26555. E. M. S. was also supported by NSF grant AST 99-01955 to Villanova University. Support was also provided by the Delaware Space Grant Colleges Consortium.

REFERENCES

- Cannizzo, J. 1998, *ApJ*, 493, 426
Froning, C. S., Long, K. S., Drew, J. E., Knigge, C. & Proga, D. 2001, *ApJ*, 562, 963
Godon, P., & Sion, E. M. 2002, *ApJ*, 566, 1084
Huang, M. et al. 1996, *ApJ*, 458, 355
Hubeny, I. 1988, *Comput. Phys. Commun.*, 52, 103
Hubeny, I., & Lanz, T. 1995, *ApJ*, 439, 875
Hubeny, I., Lanz, T., & Jeffery, C. S. 1994, in *Newsletter on Analysis of Astronomical Spectra 20*, ed. C. S. Jeffery (CCP7; St. Andrews: St. Andrews Univ.), 30
Kaitchuck, R. H. 1989, *PASP*, 101, 1129
Pringle, J. 1988, *MNRAS*, 230, 159
Sion, E. M. 1995, *ApJ*, 438, 876
———. 1999, *PASP*, 111, 532
Sion, E. M., Szkody, P., Gänsicke, B., Cheng, F., LaDous, C., & Hassall, B. 2001, *ApJ*, 555, 834
Sparks, W. M., Sion, E. M., Starrfield, S. G., & Austin, S. 1993, in *Cataclysmic Variables and Related Physics*, ed. O. Regev & G. Shaviv (Bristol: IOP), 96
Verbunt, F. 1987, *A&AS*, 71, 339
Wade, R., & Hubeny, I. 1998, *ApJ*, 509, 350